Journal of Nuclear Materials 145-147 (1987) 527-533
North-Holland, Amsterdam

THE DENSITY DEPENDENCE OF NEUTRAL HYDROGEN DENSITY AND NEUTRAL HYDROGEN EMISSION FROM PLT

D.N. RUZIC [1], D.B. HEIFETZ [2] and S.A. COHEN [2]

[1] *University of Illinois, 214 NEL, 103 S. Goodwin Avenue, Urbana, IL 61801, USA*
[2] *Plasma Physics Laboratory, Princeton University, Princeton, NJ 08544, USA*

Key words: neutral transport, charge exchange, PLT

The efflux of atoms with energies greater than 10 eV from tokamaks results primarily from charge exchange. This flux is useful as a diagnostic of plasma properties such as particle transport, particle confinement, power balance, neutral density, and ion temperature. This flux also contributes to plasma contamination by sputtering of impurities from walls and limiters. We have measured the efflux of neutral hydrogen in the energy range from 10 to 2000 eV as a function of plasma parameters in the steady-state portion of ohmically heated discharges in PLT. Results have been obtained both near the main plasma limiter and far away from it. These data serve as a benchmark for comparing atomic emission during auxiliary heating and current drive. We find that the main parameter which affects the efflux is the plasma density. The total energy-integrated efflux, Γ, rises rapidly with $\bar{n}_e$ to $\Gamma = 4\times10^{15}$ cm^{-2} s^{-1} at $\bar{n}_e = 1\times10^{13}$ cm^{-3}, and then falls a factor of 2–4. The total efflux is then relatively constant with $\bar{n}_e$ up to $\bar{n}_e \approx 6\times10^{13}$ cm^{-3}. The average energy of the efflux rises from 180 eV at $\bar{n}_e = 10^{12}$ cm^{-3} to 500 eV at $\bar{n}_e = 10^{13}$ cm^{-3}. It then decreases to approximately 150 eV at $\bar{n}_e = 2\times10^{13}$ cm^{-3}, and drops slightly more to 100 eV at $\bar{n}_e \approx 6\times10^{13}$ cm^{-3}. Using the measured $d\Gamma/dE\,d\Omega$ spectra, electron temperature, and electron density as inputs and consistency checks, the ion temperature profiles and 3-dimensional neutral density profiles are calculated using the DEGAS code. From these calculations the particle confinement time, impurity generation by sputtering, and contribution of ions and charge-exchange neutrals to the power balance are evaluated as a function of electron density. The importance of the limiter to recycling at high densities is clearly demonstrated. The ratio of the ion flux onto the limiter versus the ion flux onto the wall goes from 4.8 at $\bar{n}_e = 1.8\times10^{12}$ cm^{-3} to 6.3 at $\bar{n}_e = 1\times10^{13}$ cm^{-3}, and to 24.1 at $\bar{n}_e = 5.5\times10^{13}$ cm^{-3}.

1. Introduction

Measurement of the outflux of neutral hydrogenic atoms from tokamak plasmas has been useful in determining the central [1] and edge [2] ion temperatures. Another proposed [3] use, to determine particle confinement, is more difficult to effect experimentally because of the many detectors required to document fully the toroidally and poloidally varying flux. Such a complex array would also allow determination of the power loss and an assessment of wall sputtering by the charge-exchange hydrogen. These latter two topics are controversial. In some tokamaks [4] power accountability has never been achieved. Charge-exchange losses, particularly near the limiter, have been suggested [5] as the missing factor, but they have never been measured. Some investigations of impurity generation sites have identified the limiter [6,7] and other inboard structures [8] as the dominant impurity sources, while other investigations have identified the walls [7,9] as the dominant sources.

In this paper we combine charge-exchange flux measurements at two toroidal positions relative to a pair of fixed mushroom-type limiters using detailed computer simulations of the neutral particle transport, to evaluate particle confinement, power loss, and impurity sputtering in a range of PLT discharges. These measurements were made in ohmically-heated plasmas as a function of density, toroidal field, and plasma current. Of these three parameters, the charge-exchange efflux showed its greatest sensitivity to the plasma density, and therefore the discussion here is restricted to that parameter.

The results presented here differ from previous work [2,5,10,11] in that the range of plasma parameters studied is ten times larger, the number of discharges documented is similarly larger, the energy sensitivity of the charge exchange detector has been extended downward to one-fourth its previous lower energy threshold, and the present computer simulations are more realistic and detailed. The full importance of poloidal and toroidal variations in atomic fluxes in data interpretation will be clearly shown.

2. Experimental results

The PLT tokamak [12] is a middle sized (major radius $R = 132$ cm, minor radius $a = 40$ cm) device which operates at a line averaged electron density of $\bar{n}_e = 10^{12}$ to 10^{14} cm^{-3}, a maximum toroidal magnetic field of $B_T \approx 3.5$ T, and a maximum plasma current of $I_p \approx 700$ kA. The diagnostic used to measure the charge-exchange flux is the Low Energy Neutral Atom Spectrometer [13,15] (LENS). The LENS is capable of measuring the energy-resolved charge-exchange efflux in the range of 5 eV to 2000 eV with a time resolution of 0.2 ms. It is located at toroidal gap 3 (out of 18). Pairs of top and bottom moveable mushroom shaped limiters [14] are located at gaps 3 and 8. Any of these four limiters may serve as a main limiter if its leading edge is placed at a minor radius of approximately 40

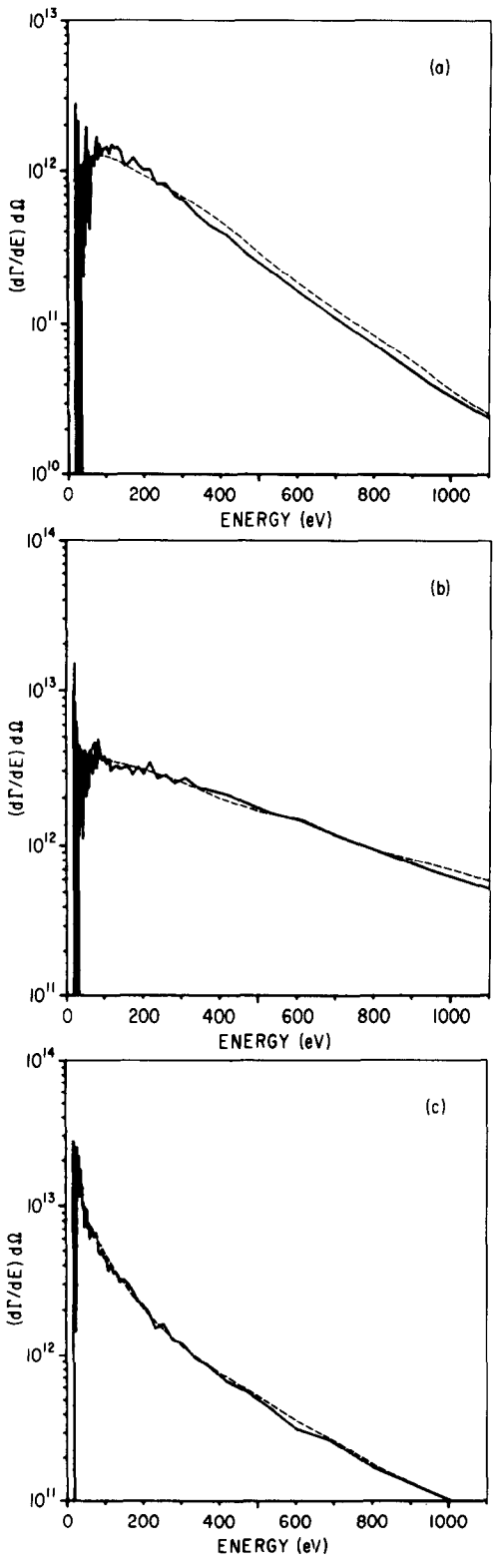

Fig. 1. The measured (solid lines) and calculated (dashed lines) charge exchange spectra $d\Gamma/dE\,d\Omega$ for the cases (a) $\bar{n}_e \approx 1.8 \times 10^{12}$ cm^{-3}, (b) 1.0×10^{13} cm^{-3}, and (c) 5.5×10^{13} cm^{-3}. The spectra were measured by the LENS detector at the toroidal position of the active limiters.

cm, while it would receive a negligible flux when withdrawn to at least a 45 cm minor radius.

The measurements were carried out during the central 400 ms of a one second duration ohmically-heated discharge. During this period the plasma parameters were in a quasi-steady state. As noted in previous publications [2,11,15], discharge initiation and termination have markedly different behavior due to the low degree of ionization, gas sources, and to the poor confinement. During the quasi-steady state, most plasma parameters, particularly B_T, are constant to a few percent. Electron densities, I_p, and the total energy integrated charge-exchange efflux are constant to about $\pm 10\%$ for at least ± 50 ms, centered at the selected measurement time. The results described below were obtained at $B_T = 1.6$ or 3.2 T, $I_p \approx 370$ kA, and $V_L \approx 1.5$ V.

Typical differential flux spectra, $d\Gamma/dE\,d\Omega$, where E is the energy, Γ is the flux, and Ω is the solid angle, for low ($\bar{n}_e \approx 1.8 \times 10^{12}$/cm^{-3}), medium ($\bar{n}_e \approx 10^{13}$/cm^{-3}), and high ($\bar{n}_e \approx 5.5 \times 10^{13}$ cm^{-3}) density discharges are shown as the solid lines in fig. 1. The line average densities quoted in this paper were obtained from the microwave interferometer. The central electron temperatures in the three discharges were 500, 1100, and 700 eV, respectively, as determined by Thomson scattering measurements. These data were acquired with the top and bottom gap 3 limiters inserted at $r = 40$ cm, and the gap 8 limiters withdrawn to $r = 45$ cm. Thus the LENS was viewing the same toroidal location as the limiter. The flux spectra were averaged over 50 ms for smoothing purposes.

At low $\bar{n}_e \approx 1.8 \times 10^{12}$ cm^{-3} (fig. 1a), the flux spectrum showed a peak at $E \approx 130$ eV, and an intensity which decreased with increasing energy in a simple exponential fashion. The tail of the spectra, $E > 300$ eV, had an effective temperature, T, of approximately 210 eV. As the density increased to $\bar{n}_e \approx 10^{13}$ cm^{-3} (fig. 1b), the total flux increased, the temperature of the tail increased to $T \approx 475$ eV, and the peak in $d\Gamma/dE\,d\Omega$ occurred at a lower energy of $E \approx 100$ eV. In the highest density case, $\bar{n}_e \approx 5.5 \times 10^{13}$ (fig. 1c), the total flux remained at about the same level as in the $\bar{n}_e \approx 10^{13}$ cm^{-3} case, however, the shape of $d\Gamma/dE\,d\Omega$ changed markedly. The tail fell rapidly, losing a simple exponential shape, and the peak signal occurred at a lower energy, $E \approx 30$ eV.

The general trend in the distributions is qualitatively understood by considering the opacity of the plasma to neutrals. At higher densities virtually all of the high energy neutrals born near the core were ionized or charge-exchanged before they make it to the wall. The peak energy qualitatively corresponds to the ion temperature of the radial position with the highest neutral density. A quantitative evaluation leading to the calculated dashed curves on fig. 1 is described in section 3.

By integrating $d\Gamma/dE\,d\Omega$ and $E\,d\Gamma/dE\,d\Omega$ over

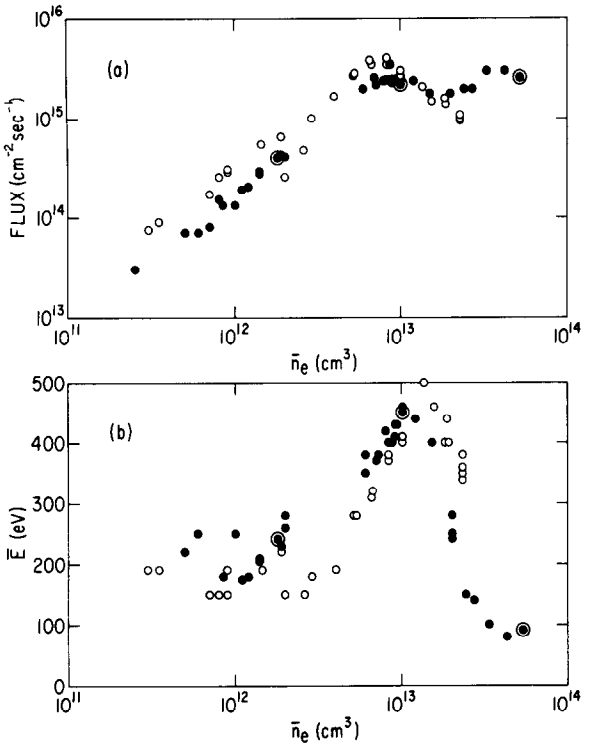

Fig. 2. (a) The total measured fluxes, Γ, and (b) average energies of the detected neutrals, $\bar{E}$, as functions of $\bar{n}_e$, for $B_T = 1.6$ T (open dots) and $B_T = 3.2$ T (closed dots).

E and Ω, the total flux, Γ, and power, P, were obtained. The average energy of these particles is then given by $\bar{E} \equiv P/\Gamma$. Both Γ and $\bar{E}$ are plotted in fig. 2 as functions of $\bar{n}_e$ for the two toroidal fields $B_T = 1.6$ T and 3.2 T. All these discharges were part of the same run, occurring within a span of four hours. The circled discharges are modelled in section 3.

As $\bar{n}_e$ increased from 3×10^{11} cm^{-3} to $\approx 8 \times 10^{12}$ cm^{-3}, the flux, Γ, increased by a factor of 100, and was approximately proportional to $(\bar{n}_e)^{1.3}$. After peaking at $\bar{n}_e \approx 8 \times 10^{12}$ cm^{-3}, the flux fell by a factor of ~ 2, and then remained constant up to the highest densities measured, implying a particle confinement time proportional to $\bar{n}_e^{-1}$. As shown in fig. 2b, the average energy of the charge-exchange particles, $\bar{E}$ also climbed as $\bar{n}_e$ increased to 10^{13} cm^{-3}. After reaching a broad peak of 450 eV, $\bar{E}$ fell precipitously at $\bar{n}_e \approx 2 \times 10^{13}$ cm^{-3} to 100 eV. This too can be qualitatively understood by considering plasma opacity. At $\bar{n}_e \approx 1$ to 2×10^{13} cm^{-3}, the mean free path of the neutrals became less than the minor radius of PLT.

Similar observations were made with the gap 3 limiters retracted to $r \geq 45$ cm and a gap 8 limiter inserted to $r = 40$ cm. The LENS then viewed the plasma 100 degrees toroidally from the functioning limiter. The major difference between data obtained in these discharges and the data in figs. 1 and 2 was the total measured fluxes were factors of 10 to 100 times lower than when the main limiter was at gap 3.

Over the past five years a total of several thousand discharges using the gap 3 and/or 8 limiters have been documented. Virtually all the ohmic heating data reproduce the behavior just described. The variation of Γ with I_p is small. Major changes occur, of course, during auxiliary heating, impurity injection, helium discharges, and small minor radius plasmas. These results will be discussed elsewhere.

3. Modelling results

Evaluating particle confinement, power loss, and impurity sputtering for the data set described in section 2 requires the interpolation and extrapolation of the charge-exchange fluxes measured at two points with respect to the rest of the torus wall. This in turn requires a detailed picture of the neutral transport, computationally done here using the DEGAS code [16].

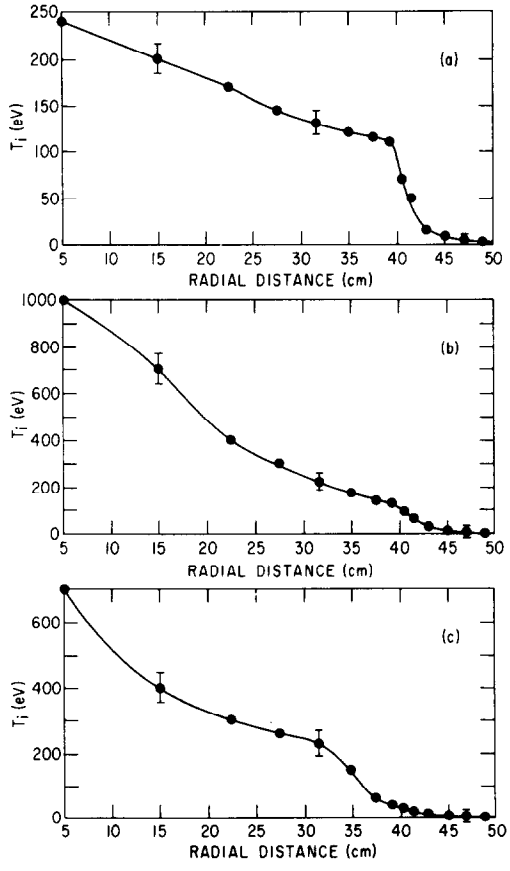

Fig. 3. Calculated ion temperature profiles for the three cases (a) $\bar{n}_e \approx 1.8 \times 10^{12}$ cm^{-3}, (b) 1×10^{13} cm^{-3}, and (c) 5.5×10^{13} cm^{-3}, calculated using the algorithm described in section 3. The points are at the 14 radial zones used in the calculation. The vertical bars are estimated uncertainties in the results at representative points.

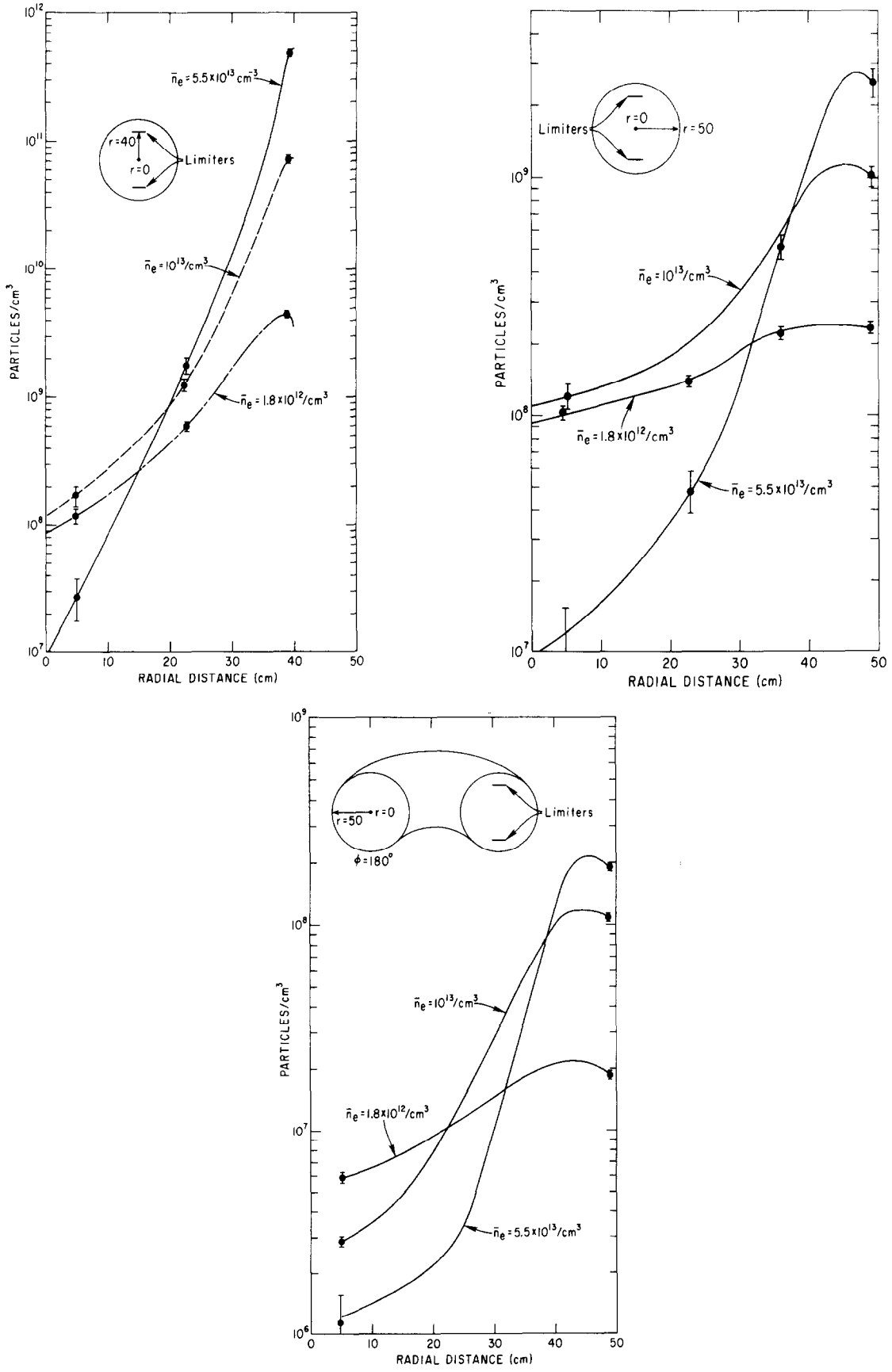

Fig. 4. Calculated n_{D^0} radial profiles for the three plasma densities perpendicular to the midplane through the limiters at $\phi = 0°$ (a), through the midplane at $\phi = 0°$ (b), and toroidally opposite from the limiter at $\phi = 180°$ (c). The vertical bars are standard errors of

DEGAS computes neutral transport in three-dimensions using Monte Carlo methods. This code includes a detailed description of the ionization, charge exchange, and plasma recombination processes, as well as wall reflection and physical sputtering. The model geometry is fully three dimensional, and includes faithful representations of the limiter and LENS geometries.

The fixed inputs into the code known from the experiment are the electron density and temperature profiles, as well as the Z_{eff} obtained from Thomson scattering, and $\mathrm{d}\Gamma/\mathrm{d}E\,\mathrm{d}\Omega$ from the two charge exchange analyzer positions relative to the active limiters. The ion temperature profile, $T_i(r)$, is initially estimated. A three-dimensional neutral density profile, $n_{D^0}(r)$, is then generated by DEGAS. Three sources of neutrals are considered: recombination of ions into atoms or molecules at the limiter surface, recombination of ions into atoms and molecules at the wall, and recombination of ions and electrons within the plasma. The third source, plasma recombination, is fixed, as it depends on the $n_i(r)$, $n_e(r)$, and $T_e(r)$ profiles only. The strengths of the first two sources and $T_i(r)$ are varied to fit the measured $\mathrm{d}\Gamma/\mathrm{d}E\,\mathrm{d}\Omega$ spectra at the two observation positions near and away from the active limiters.

After several iterations of $T_i(r)$ changes and calculations of $n_{D^0}(r)$, an agreement to within $\pm 20\%$ is obtained over the energy range of from 20 eV to 2000 eV. The $T_i(r)$ and $n_{D^0}(r)$ profiles thus produced are not in general numerically unique solutions, but are unique if the n_e and T_e profiles decrease monotonically from the axis. Doppler broadening spectroscopic measurements of $T_i(r)$ do show general agreement. Computed $T_i(r)$ profiles for the three $\bar{n}_e$ cases are shown in fig. 3. The resulting $\mathrm{d}\Gamma/\mathrm{d}E\,\mathrm{d}\Omega$ curves are shown as dotted lines in fig. 1 overlaying the experimentally obtained spectra.

Computed neutral density profiles $n_0(r, \phi, \theta)$ as functions of radial position, r, toroidal angle, ϕ, and poloidal angle, θ, are shown in figs. 4–6 for the three plasma density cases. These plots demonstrate the asymmetries in the neutral density due to the recycling at the limiter.

Fig. 4 shows the radial variations of the calculated neutral densities at the toroidal position of the limiter, $\phi = 0°$, (a) both perpendicular to the midplane ($\theta =$

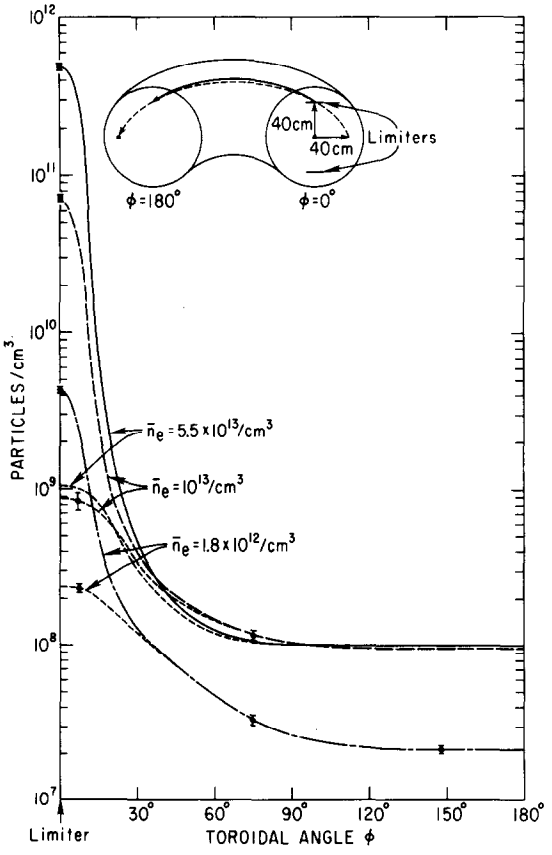

Fig. 5. Calculated n_{D^0} toroidal variation at $r = 40$ cm around the midplane ($\theta = 0°$) (solid lines), and at $\theta = 90°$ (dashed lines). The vertical bars are standard errors of the computed results at representative points.

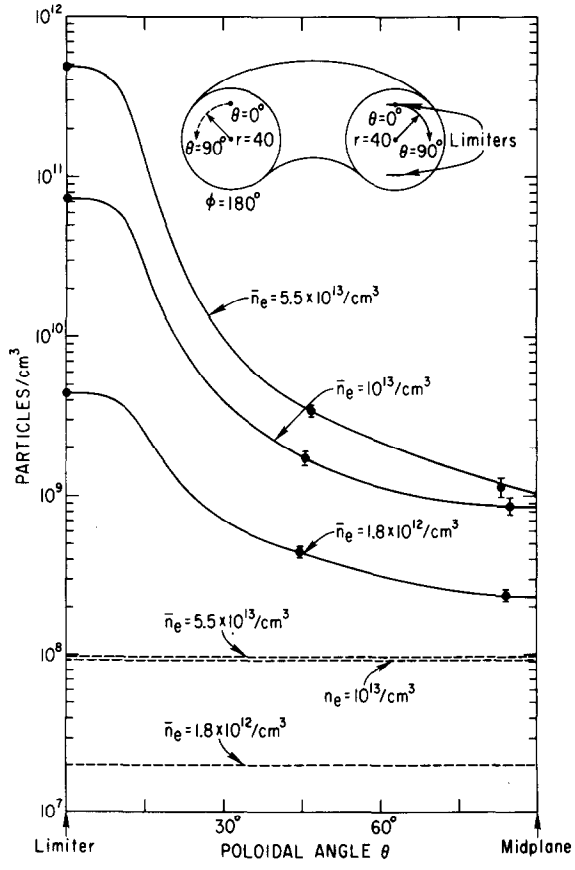

Fig. 6. Calculated n_{D^0} poloidal variation at $r = 40$ cm, for $\phi = 0°$ (solid lines) and $\phi = 180°$ (dashed lines). The vertical bars are standard errors of the computed results at representative points.

90°), and (b) through the midplane ($\theta = 0°$), and (c) toroidally opposite from the limiters, at $\phi = 180°$. The neutral populations at the limiter position are due mainly to plasma recycling off the limiters. These populations are localized to the limiter region and the populations toroidally opposite to the limiters are due almost entirely to plasma recycling at the wall. At the highest density, $\bar{n}_e \approx 5.5 \times 10^{13}$ cm^{-3}, plasma recombination is the main contributor to the neutral density in the central 10 cm. Recombination has a negligible effect on n_0 at lower densities.

The variations of the neutral densities at $r = 40$ cm with toroidal angle $\phi = 0$–$180°$ at the poloidal position of the limiter ($\theta = 90°$), and at the midplane ($\theta = 0°$), are plotted in fig. 5. In each plasma density case the neutral population at the midplane was an order of magnitude higher at $\phi = 0°$ than it was at $\phi = 180°$. The drop in neutral density toroidally at the limiter's poloidal position was even greater, decreasing, for example, in the high plasma density case from 4.9×10^{11} ($\pm 2\%$) cm^{-3} at $\phi = 0°$ to 10^8 ($\pm 14\%$) cm^{-3} at $\phi = 180°$.

Finally the neutral densities at $r = 40$ cm for poloidal angles $\theta = 0$–$90°$ at the toroidal positions $\phi = 0°$ and $\phi = 180°$ are shown in fig. 6. Away from the limiter, at $\phi = 180°$, the neutral populations did not vary poloidally, as the influence of the limiter did not extend that far. At the limiter, $\phi = 0°$, the neutral densities at $\theta = 0°$ were 1–2 orders of magnitude lower than they were at $\theta = 90°$.

Not shown in figs. 4–6 is the sensitivity of n_{D^0} to the limiter radial position. For the medium density case we have studied this and found that a ± 5 cm shift in limiter radius scales the radial profile such that the peak still occurred at the limiter radius and changed $n_{D^0}(a, 0°, 90°)$ by very little, while changing $n_{D^0}(a, 0°, 0°)$ by a factor of 3. Also the toroidal fall-off of neutral density was faster as the distance between the wall and the limiter was decreased.

Neutral molecules were even more confined to the limiter region than atoms, due to their low initial desorption velocity. The neutral molecular density, $n_{D_2^0}$, at the limiter in the high $\bar{n}_e$ case was 1.23×10^{12} ($\pm 2\%$) cm^{-3}. At the midplane limiter position, $n_{D_2^0}(40$ cm, 0°, 0°) was a factor of ~1100 lower, versus a drop in n_{D^0} of ~500 between the same two points. Toroidally opposite from the limiter, $n_{D_2^0}$ was down by a factor of $\sim 1.3 \times 10^4$ from the peak limiter value, but n_{D^0} dropped by only ~5000 over the same range. There were no molecules at the plasma center.

The localization of molecules became more pronounced in the lower $\bar{n}_e$ cases. In the lowest density case, for example, the ratio of $n_{D_2^0}$ (40 cm, 0°, 90°) to $n_{D_2^0}(40$ cm, 0°, 0°) was ~250, but the ratio of n_{D^0} (40 cm, 0°, 90°) to n_{D^0} (40 cm, 0°, 0°) was only ~22. The reason for this increased localization is that even at the lowest density, the mean free path length for molecules was only about one centimeter. Thus while the atoms were free to travel quite far from the limiter, the molecules were still confined there.

4. Discussion

The fluxes computed by the DEGAS program varied linearly with the ion currents onto the limiter, $\dot{N}_L^+$, and wall, $\dot{N}_W^+$. Thus by matching the measured neutral flux, Γ, with the calculated flux the ion currents are easily determined. The results for the three density cases are listed in table 1, along with the corresponding ion confinement times within the limiter's minor radius, τ_L^+, and the wall's minor radius, τ_W^+, and the total confinement time τ_T^+, derived from

$$\frac{1}{\tau_T^+} = \frac{1}{\tau_L^+} + \frac{1}{\tau_W^+}.$$

Both of the ion flows $\dot{N}_L^+$ and $\dot{N}_W^+$ increased with $\bar{n}_e$, and the limiter ion confinement time, τ_L^+, decreased with $\bar{n}_e$. The wall ion confinement time, τ_W^+, also decreased as $\bar{n}_e$ increased from 1.8×10^{12} cm^{-3} to 1×10^{13} cm^{-3}, however τ_W^+ then increased when $\bar{n}_e$ rose to 5.5×10^{13} cm^{-3}. The total confinement times varied inversely with $\bar{n}_e$. The limiter recycling became more dominant as the ratios of limiter to wall ion flows increased with $\bar{n}_e$ from 4.8 at $\bar{n}_e \approx 1.8 \times 10^{12}$ cm^{-3} to 24.1 at $\bar{n}_e \approx 5.5 \times 10^{13}$ cm^{-3}.

The computed total neutral fluxes onto the limiter, $\dot{N}_L^0$, and wall, $\dot{N}_W^0$, are listed in table 2. The main limiter particle flux proved to be from ions, with $\dot{N}_L^0/\dot{N}_L^+ = 0.13$–$0.30$ over our range of $\bar{n}_e$. The largest contribution to the wall flux was from neutrals born originally at the

Table 1
Ion currents and confinement times. The limiter, $\dot{N}_L^+$, and wall, $\dot{N}_W^+$, ion currents were determined by matching calculated $d\Gamma/dE\,d\Omega$ distributions, which vary linearly with $\dot{N}^+$, with LENS measurements. The limiter, τ_L^+, and wall, τ_W^+, confinement times were computed from $\tau^+ = N^+/\dot{N}^+$, where N^+ was the total ion population within the $r = 40$ cm and 50 cm minor radii respectively

$\bar{n}_e$ (cm^{-3})	$\dot{N}_L^+$ (s^{-1})	τ_L^+ (s)	$\dot{N}_W^+$ (s^{-1})	τ_W^+ (s)	τ_T^+ (s)	$\dot{N}_L^+/\dot{N}_W^+$
1.8×10^{12}	1.5×10^{19}	0.36	3.1×10^{18}	1.85	0.30	4.8
1.0×10^{13}	1.5×10^{20}	0.17	2.4×10^{19}	1.22	0.15	6.3
5.5×10^{13}	1.0×10^{21}	0.11	4.1×10^{19}	2.90	0.10	24.1

Table 2
Computed total neutral fluxes. The total neutral fluxes were computed by the DEGAS code onto the limiter, $\dot{N}_L^0$, and wall, $\dot{N}_{L\to W}^0$, $\dot{N}_{W\to W}^0$, due to limiter and wall plasma recycling respectively. The total calculated neutral flux onto the wall is given by $\dot{N}_W^0$.

$\bar{n}_e$ (cm^{-3})	$\dot{N}_L^0$ (s^{-1})	$\dot{N}_{L\to W}^0$ (s^{-1})	$\dot{N}_{W\to W}^0$ (s^{-1})	$\dot{N}_W^0$ (s^{-1})	$\dot{N}_L^0/\dot{N}_L^+$	$\dot{N}_W^0/\dot{N}_W^+$
1.8×10^{12}	2.0×10^{18}	1.4×10^{19}	4.5×10^{18}	1.8×10^{19}	0.13	5.8
1.0×10^{13}	3.5×10^{19}	6.6×10^{19}	2.2×10^{19}	8.8×10^{19}	0.23	3.7
5.5×10^{13}	3.0×10^{20}	1.5×10^{20}	2.9×10^{19}	1.8×10^{20}	0.30	4.4

limiters, $\dot{N}_{L\to W}^0$. The ratio $\dot{N}_W^0/\dot{N}_W^+$ ranged from 3.7 to 5.8. The wall neutral fluxes from the limiter recycling were localized near the limiters. This is consistent with the localization of n_0 near the limiters discussed in section 3.

The computed power depositions onto the limiters and walls by neutral particles were negligible compared with the total experimentally measured limiter power depositions. In the highest $\bar{n}_e$ case, the total calculated power deposited by neutrals onto the limiter was 800 W. This was consistent with the computed values for the limiter neutral flux of $\dot{N}_L^0 = 3.0\times10^{20}$ particles/s, and the average energy of atoms striking the limiter of ~ 20 eV. The computed wall power from neutral particle impact in the $\bar{n}_e \approx 5.5\times10^{13}$ cm^{-3} case was only 142 W. Thus the term in the power balance from neutral impact with the wall was smaller than the power unaccounted for.

The computed values of physical erosion of the limiter and wall by both ions and neutrals are given in table 3. The main source of carbon physically sputtered off the limiter was through ion impact. Incident atoms accounted for only 3–6% of the total carbon yield. This was consistent with the high values of $\dot{N}_L^+/\dot{N}_L^0$ noted above, together with the higher ion impact energies. Note that chemically eroded CH_4 may be a larger source of carbon in the plasma due to the relatively high yields for CH_4 at high limiter temperatures. The calculated sputtering rate of iron off the wall was due almost entirely to incident atoms, because the ion struck the wall with energies below the sputtering threshold energy.

Table 3
Computed physical erosion

$\bar{n}_e$ (cm^{-3})	Limiter (carbon/s)			Wall [a] (Fe/s) neutrals
	Ions	Neutrals	Total	
1.8×10^{12}	3.3×10^{17}	8.9×10^{15}	3.4×10^{17}	1.5×10^{17}
1.0×10^{13}	3.4×10^{18}	2.1×10^{17}	3.6×10^{18}	1.4×10^{18}
5.5×10^{13}	2.2×10^{19}	1.1×10^{18}	2.3×10^{19}	1.5×10^{18}

[a] Ion sputtering of the wall was negligible.

The authors would like to thank Dr. C. Daughney for providing Thomson scattering data. This work was supported by the US Department of Energy Contract No. DE-AC-02-76-CHO-3073, and an NSF Presidential Young Investigator Grant awarded to one of the authors (D.N.R.).

References

[1] See A.I. Kislyakov and L.I. Krupnik, Sov. J. Plasma Phys 7 (1981) 478, and refs. therein.
[2] D.E. Voss and S.A. Cohen, J. Nucl. Mater. 93 & 94 (1980) 405.
[3] S.A. Cohen, in: Physics of Plasma–Wall Interactions in Controlled Fusion, Eds. D.E. Post and R. Behrisch (Plenum Press, New York, 1986).
[4] E.B. Meservey et al., J. Nucl. Mater. 93 & 94 (1980) 267.
[5] S.A. Cohen and D.E. Voss, in: Proc. Fourth Topical Conf. on the Technology of Controlled Nuclear Fusion, King of Prussia, PA. 1 (1980) 61.
[6] R.L. Isler et al., Phys. Rev. Lett. 47 (1981) 333.
[7] R.L. Isler, Nucl. Fus. 24 (1984) 1599, and refs. therein.
[8] B.C. Stratton et al., Nucl. Fusion 24 (1984) 767.
[9] J. Roth, J. Nucl. Mater. 103 & 104 (1981) 291.
[10] F. Wagner, J. Vac. Sci. and Tech. 20 (1982) 1211, and refs. therein.
[11] S.A. Cohen, D. Ruzic and D.E. Voss, Nucl. Fusion 24 (1984) 1490.
[12] D. Grove et al., Proc. Sixth Int. Conf. on Plasma Physics and Controlled Fusion Research, Vol. I (IAEA, Vienna, 1977) p. 21.
[13] D.E. Voss and S.A. Cohen, Rev. Sci. Instr. 53 (1982) 1696.
[14] S.A. Cohen, R. Budny, G.M. McCracken and M. Ulrickson, Nucl. Fusion 21 (1981) 233.
[15] D. Voss, Thesis, Princeton University (1980).
[16] D.B. Heifetz et al., J. Comp. Phys. 46 (1982) 309.